DesignCon 2013

Analytic Solutions for Periodically Loaded Transmission Line Modeling

Priya Pathmanathan, Intel Corporation
priya.pathmanathan@intel.com

Paul G. Huray, University of South Carolina
huray@sc.edu

Steven G. Pytel, ANSYS Inc.
steve.pytel@ansys.com

Abstract

The impact of periodic fiber-weave dielectric inhomogeneity on signal loss has been characterized through empirical methods in previously published literature. In this paper, we present an analytic solution for periodically loaded transmission lines to model additional losses due to periodic loading. We derive analytical equations based on Floquet-Bloch periodic wave propagation theory to predict additional transmission losses in evanescent frequency bands known as Brillouin zones in which we have treated a transmission line PCBs rotated from fiber weave fabrics as a periodic transmission medium and applied the theory to predict additional losses. Theoretical predictions have been correlated to 3D-EM simulations with complete fiber weave models and to high frequency VNA measurements up to 100GHz. One of the primary outcomes of this work is fundamental analytical formula to predict the periodic loss profile of a given periodic structure geometry. This work provides a technique for inclusion of fast analytical algorithms in high-speed signal integrity simulation models to correct for additional periodic loss mechanisms.

Author(s) Biography

Priya Pathmanathan is Senior Analog Engineer at Intel Corporation where he works on observability tools development for high-speed serial and parallel busses. He develops design specifications for silicon, packaging, and platforms to enable silicon observability. He received his Ph.D. in electrical engineering from the University of South Carolina.

Paul G. Huray is professor of electrical engineering at the University of South Carolina and has worked at the Oak Ridge National Laboratory, Intel, and the White House. Professor Huray introduced the first graduate program on signal integrity and is the author of the books ***Maxwell's Equations*** and ***The Foundations of Signal Integrity***.

Steven Gary Pytel Jr. is the Lead Signal Integrity Product Manager for the Ansoft product line. He received a Doctor of Philosophy specializing in Signal Integrity from the University of South Carolina and previously worked at Intel Corporation as a Senior Signal Integrity and Hardware Design Engineer where he helped design Blade, Telecom, and Enterprise servers. His current research interests include high speed serial signaling, statistical analysis of digital circuits, and hybrid electromagnetic field solvers.

Introduction

Ever increasing digital signaling rates with faster rise and fall times, in accordance with Moore's Law, demand higher and higher bandwidths from system interconnects, often in the sub millimeter wavelength regime. Therefore, understanding propagation properties and controlling loss mechanisms of interconnects is becoming critical to maintain the Signal Integrity (SI) of busses carrying critical digital data.

Printed Circuit boards (PCBs), packages, flex cables, and connectors are the common interconnecting medium for modern computer systems that communicate between various processors and chipsets. Typical PCB manufacturing processes embed layers of woven fiberglass cloth in resins to mechanically strengthen the PCB. Generally the fiberglass and resin have different electrical properties including dielectric strengths and constants. This difference creates a periodically loaded dielectric medium. PCB construction is not the only source of periodic loading in modern high speed signal interconnects. Routing through a pin grid array, placing surface mount discrete components near a signal net within a PCB or package, and braided shielding on cables are a few examples where periodic loading could potentially affect the signal integrity.

In recent years, micro-scale (PCB) effects such as surface roughness and fiber weave effect have received closer attention. This is mainly due to the adverse impacts on loss characteristics of microstrip and stripline traces introduced by these effects at higher frequencies. Resonance effects on insertion and return loss profiles of PCB traces were observed several years ago but remained an unexplained mystery for a long time. Recently these resonances were verified through controlled experiments to rule out several possible factors including humidity effects, structural defects, and measurement equipment errors, as potential causes for these resonances [1]. Figure 1 shows the fiber weave resonances of a stripline test board recorded by researchers at Intel and the University of South Carolina.

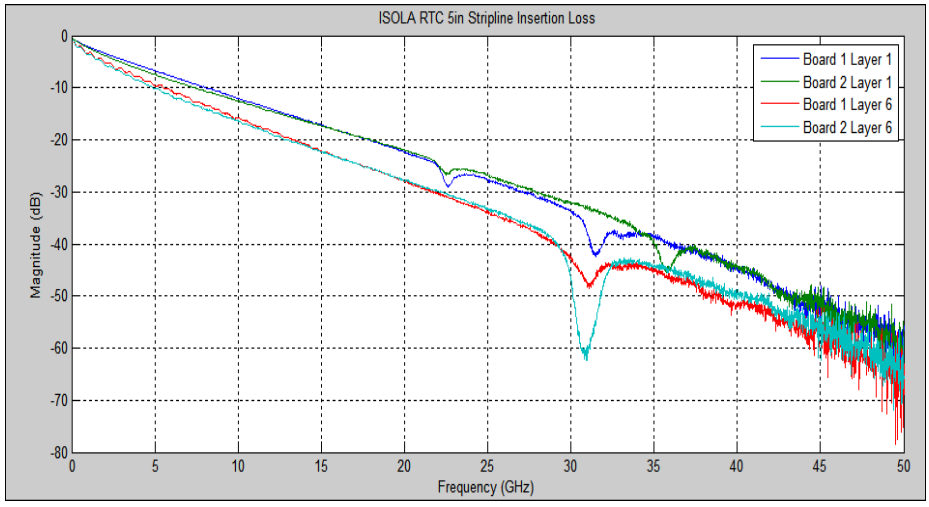

Figure 1 VNA Measurement of Insertion Loss on ISOLA 620 RTC Test Boards

Periodic loading effects due to fiber weave structure were identified as the cause for the resonances at certain frequencies and attempts were made to correlate the measurements to complete 3D electromagnetic field solvers[2][3]. For digital signaling channels operating at very high data rates (16GT/s and above) these periodically occurring discontinuities can cause large signal attenuation in certain stop band frequency regimes. The attenuation, in addition to conductor and dielectric losses, can dominate channel performance in certain frequency bands. These effects must be included in simulation models to yield accurate system simulation results. Currently available techniques [4] can predict the resonance frequency based on the multi-cell periodicity [MCP] of a rotated routing on a PCB. However, the usefulness of this technique is limited to simulation modeling applications, because of the fundamental assumption that a fiber weave medium can be approximated to a uniform dielectric medium. Effective dielectric constant is computed as a weighted average of glass and resin dielectric constant in these techniques. Because of this limitation, current techniques cannot be applied to predict the amplitude or bandwidth of the resonance.

Analytical Approach

Characterizing PCB transmission lines using parameterized models for dielectric and conductor loss is popular within the Signal Integrity (SI) community. Signal Integrity Simulation models can be generated using 3D EM simulations, measurements, and analytical techniques. However, measurements and 3D EM simulations alone are not practical for modeling micro scale periodic effects at a system scale. Measurements require high bandwidth equipment and test fixtures to accurately characterize the loss profiles. 3D EM simulations in many cases are also not practical due to the demand for a large amount of computing resources. Solutions to wave equations in a periodic dielectric medium were previously presented in [2] and [3]. This paper explains another, more practical, approach to the same problem. This paper introduces fundamental periodic transmission line theory and its application to transmission line modeling with special focus on fiber weave structures within a PCB. Proposed analytical techniques, combined with 3D simulations and/or measurements, can be employed to generate scalable models which accurately predict the additional losses due to periodic loading in transmission media. This theory can be extended beyond fiber weaves to any periodic loading conditions often observed in signal interconnects, such as routings through a Pin Grid Array (PGA).

Below, we explain the fundamental theory by considering a Periodic Transmission line as a cascaded structure of unit cells characterized as an ABCD matrix. We apply the Floquet-Bloch theorem to form an eigen-value relation for periodic conditions. Evanescent frequency regions will be identified from the dispersion relation. We use the Chebyshev Identity to derive the N^{th} power of a reciprocal ABCD matrix to cascade

similar ABCD matrices. This analytic approach will be validated with a simple S-parameter simulation using a SPICE simulator.

We also propose schemes to approximate fiber weave geometry as a periodic unit cell. Periodic unit cells will be individually characterized by 3D-EM field solvers and additional periodic resonances are analytically computed with the aid of the developed theory. We also solve a complete 3D fiber weave model and compare the analytical predictions to complete full wave EM simulations. This will demonstrate the effectiveness in modeling by characterizing just a single unit cell to create scalable transmission line models with periodic loading.

Periodic Transmission Line theory

Wave propagation in one-dimensional periodic medium with two alternatively repeating materials is analogous to a wave propagating along a periodic transmission line composed of two discrete transmission line segments with different transmission characteristics. Equivalent transmission-line modeling is preferred to model PCB traces, which often support TEM and quasi-TEM modes of propagation. Using well-established measurement and simulation techniques, smaller homogeneous sections of the periodic unit cell can be characterized as a transmission line with characteristic impedance and a complex propagation constant. It is also common practice to characterize the transmission lines with R, L, G, and C quantities per unit length.

Figure 2 illustrates a two tone periodic transmission line composed of two types of transmission lines 1 and 2 characterized by unit length quantities of {R1,L1,G1,C1} and {R2,L2,G2,C2} respectively. Figure 3 defines a unit-cell with current and voltage measurement points (with respect to a common ground).

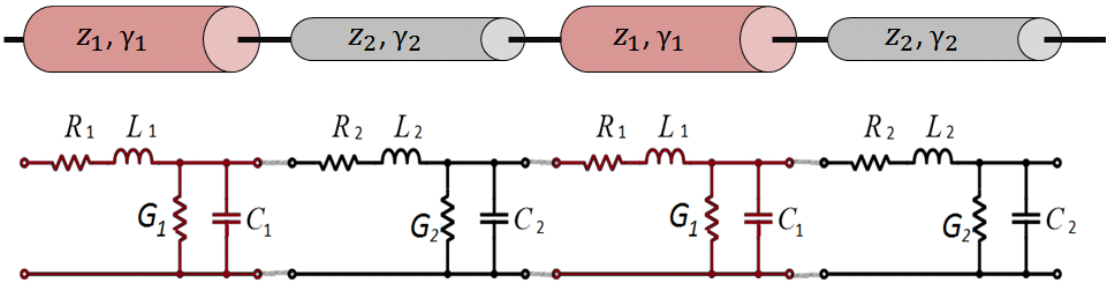

Figure 2. A Two Tone Periodic Transmission Line

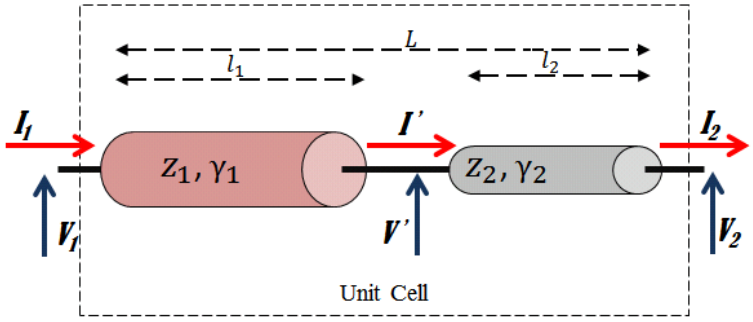

Figure 3. Current and Voltage Definitions for a Periodic Unit-cell.

Characteristic impedances and complex propagation constants of elementary transmission lines of the unit-cell can be expressed in terms of R, L, G, and C parameters [9] as

$$Z_1 = \sqrt{\frac{R_1 + j\omega L_1}{G_1 + j\omega C_1}} \tag{1}$$

$$Z_2 = \sqrt{\frac{R_2 + j\omega L_2}{G_2 + j\omega C_2}} \tag{2}$$

$$\gamma_1 = \sqrt{(R_1 + j\omega L_1)(G_1 + j\omega C_1)} \tag{3}$$

$$\gamma_2 = \sqrt{(R_2 + j\omega L_2)(G_2 + j\omega C_2)} \tag{4}$$

ABCD parameters for lossy transmission lines can be written for each elementary section as

$$\begin{matrix} A_1 & B_1 \\ C_1 & D_1 \end{matrix} = \begin{matrix} \cosh\gamma_1 l_1 & Z_1 \sinh\gamma_1 l_1 \\ \frac{\sinh\gamma_1 l_1}{Z_1} & \cosh\gamma_1 l_1 \end{matrix} \tag{5}$$

$$\begin{matrix} A_2 & B_2 \\ C_2 & D_2 \end{matrix} = \begin{matrix} \cosh\gamma_2 l_2 & Z_2 \sinh\gamma_2 l_2 \\ \frac{\sinh\gamma_2 l_2}{Z_2} & \cosh\gamma_2 l_2 \end{matrix} \tag{6}$$

Voltages and currents of the unit-cell as defined in Figure 3 can be related using *ABCD* parameters as

$$\begin{matrix} V_1 \\ I_1 \end{matrix} = \begin{matrix} A_1 & B_1 \\ C_1 & D_1 \end{matrix} \begin{matrix} V' \\ I' \end{matrix} \tag{7}$$

$$\begin{matrix} V' \\ I' \end{matrix} = \begin{matrix} A_2 & B_2 & V_2 \\ C_2 & D_2 & I_2 \end{matrix} \tag{8}$$

Eliminating V' and I' from Equations (7) and (8), yields

$$\begin{matrix} V_1 \\ I_1 \end{matrix} = \begin{matrix} A_1 & B_1 & A_2 & B_2 & V_2 \\ C_1 & D_1 & C_2 & D_2 & I_2 \end{matrix} \tag{9}$$

By definition of *ABCD* parameters, Equation (9) forms a combined *ABCD* matrix for the whole unit-cell. The combined *ABCD* matrix is given by

$$\begin{matrix} A & B \\ C & D \end{matrix} = \begin{matrix} A_1 & B_1 & A_2 & B_2 \\ C_1 & D_1 & C_2 & D_2 \end{matrix} \tag{10}$$

Generalizing the above result to an arbitrary nth unit cell with ports ”n” and “n-1” yields a relationship between the voltages and currents of port ”n” and port “n-1” linked by an ABCD matrix as expressed by equation(11)

$$\begin{matrix} V_{n-1} \\ I_{n-1} \end{matrix} = \begin{matrix} A & B & V_n \\ C & D & I_n \end{matrix} \tag{11}$$

where A, B, C and D parameters are given by

$$A = \cosh\gamma_1 l_1 \cosh\gamma_2 l_2 + \frac{Z_1}{Z_2}\sinh\gamma_1 l_1 \sinh\gamma_2 l_2 \tag{12}$$

$$D = \cosh\gamma_1 l_1 \cosh\gamma_2 l_2 + \frac{Z_2}{Z_1}\sinh\gamma_1 l_1 \sinh\gamma_2 l_2 \tag{13}$$

$$B = Z_2 \cosh\gamma_1 l_1 \sinh\gamma_2 l_2 + Z_1 \sinh\gamma_1 l_1 \cosh\gamma_2 l_2 \tag{14}$$

$$C = \frac{1}{Z_1}\sinh\gamma_1 l_1 \cosh\gamma_2 l_2 + \frac{1}{Z_2}\cosh\gamma_1 l_1 \sinh\gamma_2 l_2 \tag{15}$$

Floquet-Bloch Theorem for Periodic Medium

Floquet's theorem is a fundamental theorem explaining the concept of wave propagation in periodic media [5]. Floquet’s theorem states that if F(z) represents a wave propagating in positive z direction of a periodic medium with periodicity p, then the following condition must be satisfied:

$$F(z+p) = e^{-\gamma p} F(z) \tag{16}$$

where γ is the periodic propagation constant. In general, the solution for γ may be complex. Real and imaginary parts of γ determine attenuation and propagation properties introduced by the periodic structure. Electric field intensity components in an infinite periodic medium with a periodic pitch of L satisfies

$$E_k\ x + L\ = E_k\ x \tag{17}$$

We can apply Floquet's result to relate currents and voltages separated by the period L as in equation (9) at the ports of the periodic unit-cell with an introduction of Bloch Wave Number k.

$$\begin{matrix} A & B \\ C & D \end{matrix} \begin{matrix} V_2 \\ I_2 \end{matrix} = e^{\pm jkL} \begin{matrix} V_2 \\ I_2 \end{matrix} \tag{18}$$

In equation (18) $e^{\pm jkL}$ is the eigenvalue of the *ABCD* matrix. We can further simplify this as

$$\begin{matrix} A - e^{\pm jkL} & B \\ C & D - e^{\pm jkL} \end{matrix} \begin{matrix} V_2 \\ I_2 \end{matrix} = 0 \tag{19}$$

$$e^{\pm 2jkL} - \ A + D\ e^{\pm jkL} + AD - BC = 0 \tag{20}$$

Assuming these transmission lines are reciprocal, we can apply the reciprocal property of the ABCD matrix which is given by$AD - BC = 1$.

$$e^{\pm 2jkL} - \ A + D\ e^{\pm jkL} + 1 = 0 \tag{21}$$

The sum of the roots of this quadratic function is

$$A + D\ = \ e^{jkL} + e^{-jkL} = 2Cos(kL) \tag{22}$$

$$\frac{A+D}{2} = \cos kL = \cosh \gamma_1 l_1 \cosh \gamma_2 l_2 + \frac{1}{2}\ \frac{Z_2}{Z_1} + \frac{Z_1}{Z_2}\ \sinh \gamma_1 l_1 \sinh \gamma_2 l_2 \tag{23}$$

Bloch wave number k can be expressed as an inverse cosine function as in Equation (24)

$$k = \frac{1}{L} \cos^{-1}\ \frac{A+D}{2} \tag{24}$$

This relation is also known as the Dispersion Relation. Expressing dispersion relation between k and ω as an inverse cosine function gives an intuitive understanding of the

characteristics of this propagation constant. When $\frac{1}{2}(A+D) \leq 1$, k is real and the waves are propagating. When $\frac{1}{2}(A+D) > 1$, k becomes imaginary and the wave is evanescent.

$$\frac{1}{2}(A+D) = 1 \tag{25}$$

The expression (25) thus defines band edges and bandwidth, in which wave propagation due to periodic condition is evanescent. Evanescent frequency bands defined by these boundaries are known as Forbidden Bands or Brillouin Zones.

This phenomenon of frequency-dependent propagation loss properties of periodic mediums were well studied in the twentieth century with a focus on crystalline structures and Bragg diffraction. Léon Brillouin studied periodic wave propagation in greater details and introduced this concept which was referred to as Brillouin Zones in honor of this French physicist. Since then, several researchers have analyzed electromagnetic and generic wave propagation in detail. Recently, researchers have been studying periodic metal structures with a focus on antenna array applications and Electronic Band Gap (EBG) filter applications. However, there have been no theoretical studies done to understand the periodic structures encountered in digital signal transmission channels and their implications to the Signal Integrity of System Busses.

Figure 4 is an example plot of dispersion relation (24) between normalized k (K) and normalized ω ($2\pi f$) for an arbitrary selected periodic transmission line structure with unit cell parameters of $Z0_1 = 45\Omega$, $TD_1 = 12ps$ and $Z0_2 = 55\Omega$, $TD_2 = 15ps$. A loss-free, ideal transmission lines was assumed ($R = G = 0$) in this example for simplicity. The shaded regions of Figure 4 are the Brillouin Zones where the imaginary part of K is not zero. This selected example demonstrates several possible dispersion zones with non-equal bandwidths and amplitudes in the frequency range of 0 to 100GHz.

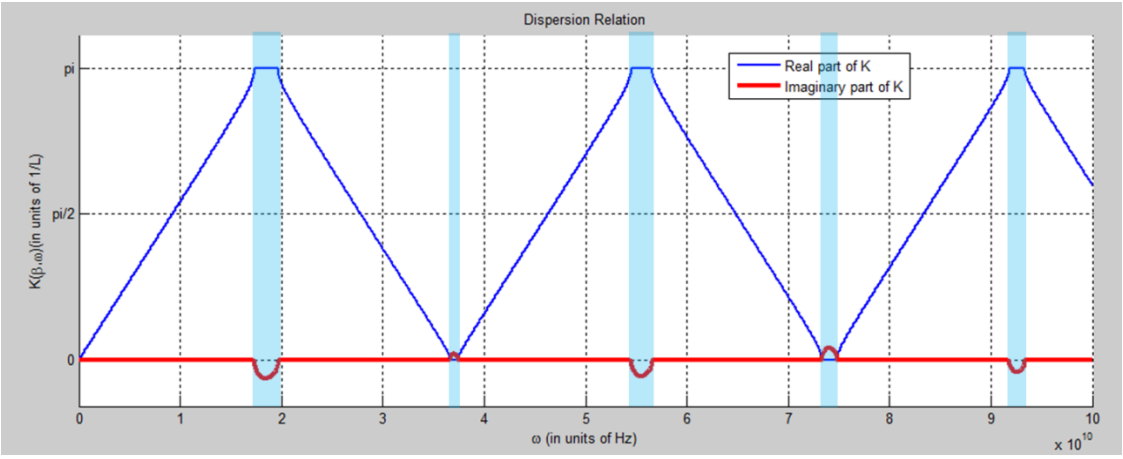

Figure 4. Dispersion Relation between *K* and ω of a periodic T-line model.

Cascading Periodic Unit-Cells of a Finite Periodic Structure

In the previous section, we established the solution for dispersion band edges for an infinitely long medium. However, real world problems are bound to a finite length structure. Exact solutions for the magnitude of losses within the dispersion zone can be derived by cascading the *N* number of identical ABCD matrices. Cascading ABCD matrices can be achieved by linear multiplication to yield N^{th} power of the single ABCD parameter.

Since $\begin{matrix} A & B \\ C & D \end{matrix}$ is a reciprocal matrix, the N^{th} power of it can be simplified using the Chebyshev Identity [6] defined by equations (26),(27), and (28). This identity can be verified using the method of induction[8]

$$\begin{matrix} A & B \\ C & D \end{matrix}^{N} = \begin{matrix} AU_{N-1} - U_{N-2} & BU_{N-1} \\ CU_{N-1} & DU_{N-1} - U_{N-2} \end{matrix} \tag{26}$$

where

$$U_N = \frac{\sin(N+1)KL}{\sin KL} \tag{27}$$

and

$$\cos(\mathrm{KL}) = \frac{\mathrm{A} + \mathrm{D}}{2} \tag{28}$$

With the above results, transfer matrix connecting voltages and currents at both ports of the transmission line can be written as in Equation (29)

$$\begin{matrix} V_0 \\ I_0 \end{matrix} = \begin{matrix} AU_{N-1} - U_{N-2} & BU_{N-1} & V_N \\ CU_{N-1} & DU_{N-1} - U_{N-2} & I_N \end{matrix} \tag{29}$$

Equation (29) completes the solution to periodic loading in a finite transmission line with an ABCD parameter, which is a complete analytical solution to dispersion zones due to periodic loading in terms of periodic geometric and electrical parameters.

Scattering Parameters

S-parameters (scattering parameters) are often preferred when characterizing transmission mediums. They more accurately characterize measured networks by relating the reflected power as a fraction of delivered power[10]. S-parameters of a finite medium in the previous section can be directly obtained by converting the ABCD matrix in Equation (29) into S-parameters with reference to the characteristic impedance of Z0. A two-port periodic S-parameter of finite length with a reciprocal structure that has N

periods can be expressed as shown in Equations (30) and (31). Note that these quantities represent loss of the structure due to periodic the loading only.

$$SP_{11} = \frac{(AU_{N-1} - U_{N-2}) + \frac{BU_{N-1}}{Z_0} - CU_{N-1}Z_0 - (DU_{N-1} - U_{N-2})}{(AU_{N-1} - U_{N-2}) + \frac{BU_{N-1}}{Z_0} + CU_{N-1}Z_0 + (DU_{N-1} - U_{N-2})} \quad (30)$$

$$SP_{21} = \frac{2}{(AU_{N-1} - U_{N-2}) + \frac{BU_{N-1}}{Z_0} + CU_{N-1}Z_0 + (DU_{N-1} - U_{N-2})} \quad (31)$$

Insertion loss (S_{21}) is a measure of the square root of the ratio of power transmitted P($x=l$) through a port at a distance L to the power injected P($x=0$) at the reference port.

$$S_{21}\ \omega\ = \ \overline{\frac{P_{(l)}}{P_{(0)}}} = \ 10^{-\alpha_{dB}\frac{l}{20}} \quad (32)$$

where α_{dB} is the attenuation coefficient. α_{dB} represents a combination of losses caused by various factors such as dielectric loss, impurities in materials, surface roughness of the conductors, and periodic loss. We can separate these loss contributions, as in Equation (33) and use it as a metric to evaluate periodic losses as a function of frequency, ω. Equation (32) derived in the previous section can be used to evaluate the periodic contribution by $\alpha_{periodic}$.

$$S_{21}\ \omega\ = \ 10^{-\alpha_{dielec.}\frac{l}{20}} \quad 10^{-\alpha_{rough}\frac{l}{20}} \quad 10^{-\alpha_{impuriy}\frac{l}{20}} \quad 10^{-\alpha_{periodic}\frac{l}{20}} \quad (33)$$

From equation (31) it is evident that the insertion losses within stop band regimes are not linearly scaling with number of periods *N*. Generally, insertation loss is assumed linearly scalable with the length for signal integrity modeling practices due to limited simulation and measurements resources. However, this assumption is only valid outside the stop bands. Loss inside stop bands can be analytically characterized for a given length of the structure according to Equation (31).

Simulation Verification

A simple SPICE simulation was performed as an example to verify the theory outlined above. In this example, the unit cell structure ($Z0_1 = 45\Omega$, $TD_1 = 12ps$ and $Z0_2 = 55\Omega$, $TD_2 = 15ps.$) assumed in Figure 4 was modeled using ANSYS® Designer®. Single ended S-parameter simulations were performed up to 100GHz on a structure with twelve (*N*=12) cascaded unit-cells. Results of the simulations are plotted in Figure 5 as insertion and return loss parameters. We can clearly see the deep resonances within the stop bands theoretically identified in Figure 4.

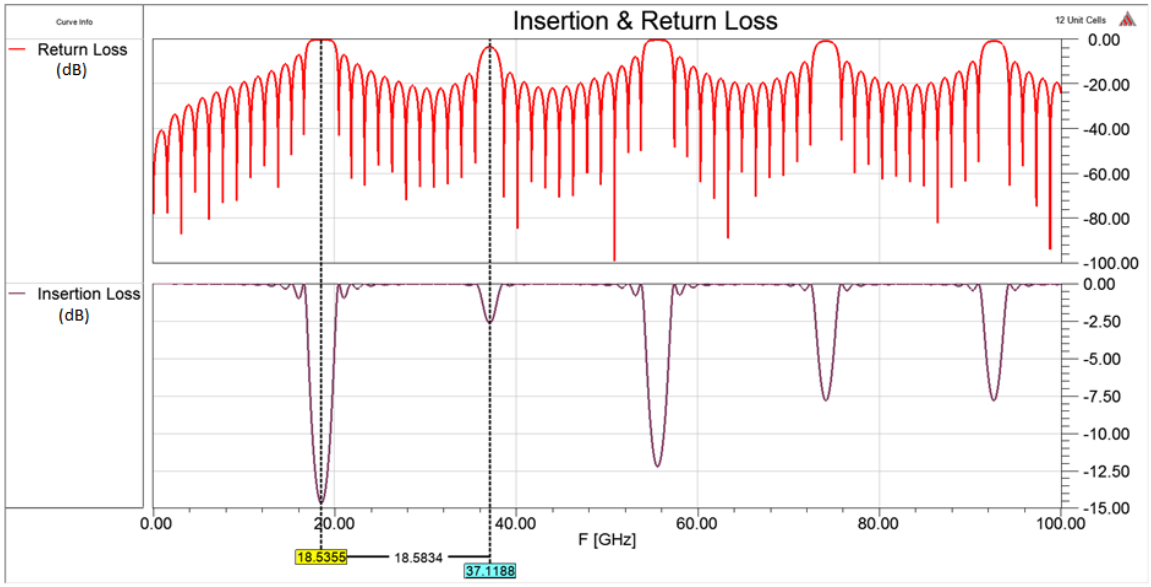

Figure 5. Return and Insertion loss profiles of 12-cell Periodic line: Spice Simulation

Figure 6 shows the insertion loss profile of the same twelve-cell periodic structure computed using a Matlab® code to compute S_{21} using Equation (31) for frequencies up to 100GHz. Insertion loss profiles of Figure 5 and Figure 6 shows a match in terms of Brillion zone bandwidths and peak amplitudes. Thus, the presented theory is verified with SPICE simulations. It also important to note the side lobes around main resonances are also matched. An analytical formula gives an exact solution for these side-lobes, which are hard to measure using lab equipment.

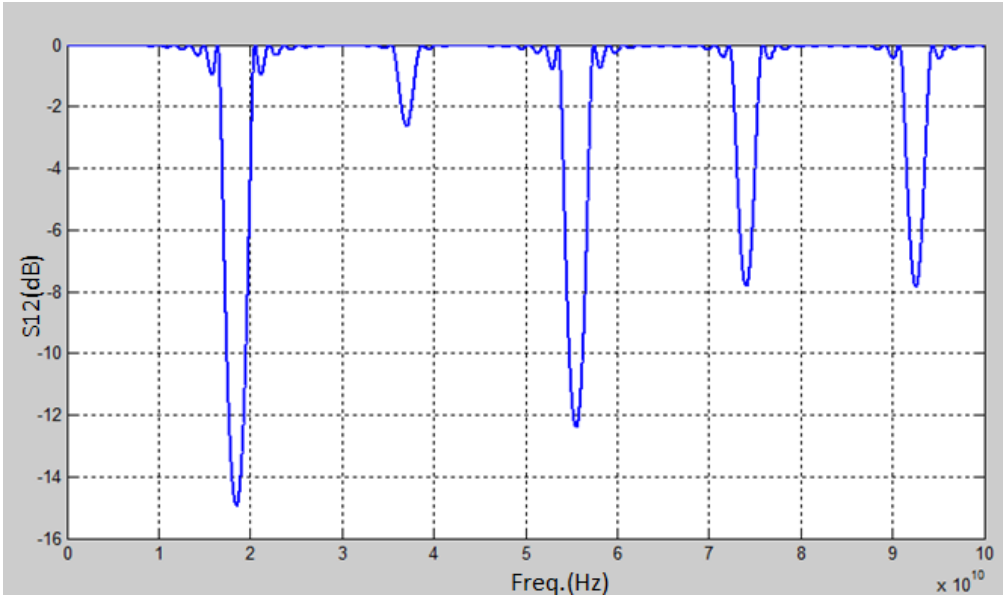

Figure 6. Insertion loss profile of 12-cell periodic line: Analytical Computation

Fiber Weave Modeling

The theory outlined in the previous section can be ubiquitously applied to any periodic structure, which can be approximated to a unit cell with two distinct transmission line models. Some examples of applications include fiber weave structures and routing through a BGA pin-field. In this section, we will discuss the use of a 3D full wave FEM EM field solver to model and analyze the fiber weave resonances. We will also apply the periodic transmission line theory to selected fiber weave geometries, and correlate to 3D EM simulations and measurements. All 3D EM simulations were performed using ANSYS® HFSS® version 14.

3D EM Field Solver Simulations and Measurements

In order to correlate our theoretical predictions to real world observations, we have created prepreg models with fiber weaves as elliptical cross-sectional bundles. Wefts and wraps were modeled as sinusoidal weaves by sweeping appropriate elliptical cross-section planes along a sinusoidal curve [7]. A 3D model of a microstrip trace on a 2116 type fiber weave is shown as an example in Figure 7.

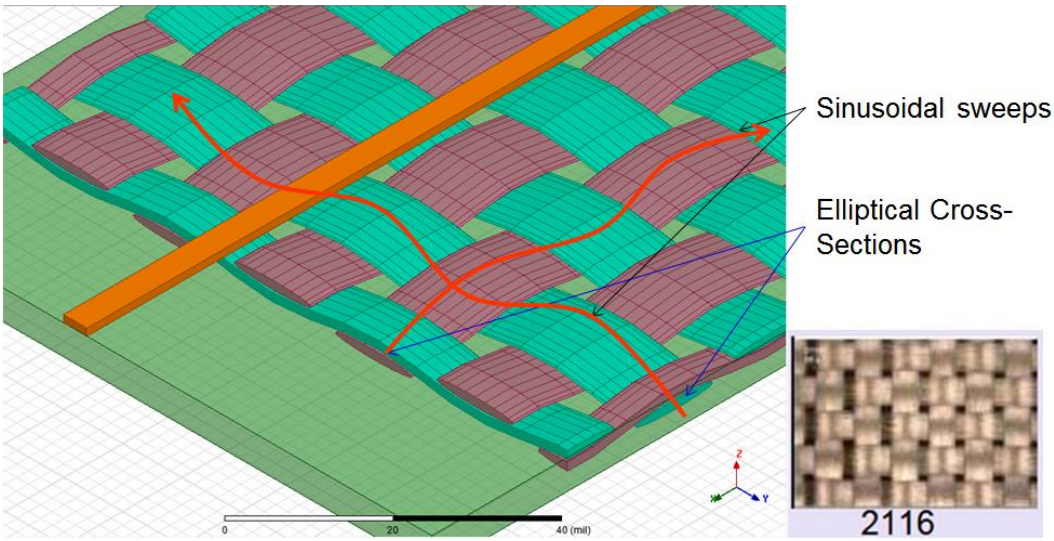

Figure 7 . Accurate Fiber Weave Model of type 2116

Stripline models were created to match our test board stackup parameters. Our test board routings were rotated by 10 degrees with respect to the fiber weave geometry. As an experiment we simulated both orthogonal and 10 degree rotated models to drive S-parameters. As presented in [4] and [3] resonances on orthogonal routings due to Single Cell Periodicity (SCP) were observed well above 110 GHz only but resonances due to Multi Cell Periodicity (MCP) were observed in the neighborhood of 20GHz to 40GHz depending on weave type. Since only MCP is the cause for the resonances in the frequency ranges of interest, we will limit the discussion to MCP for a 10 degree rotation.

Figure 8 illustrates two possible routing schemes of a microstrip, which was instructed to be routed as a 10-degree rotated routing on a 1080 prepreg. Depending on how the boards are fabricated it is possible to have two distinct MCP geometries as in Figure 8(a) (which is a rotated at 10^0) and Figure 8(b) (which is a rotated at 80^0)

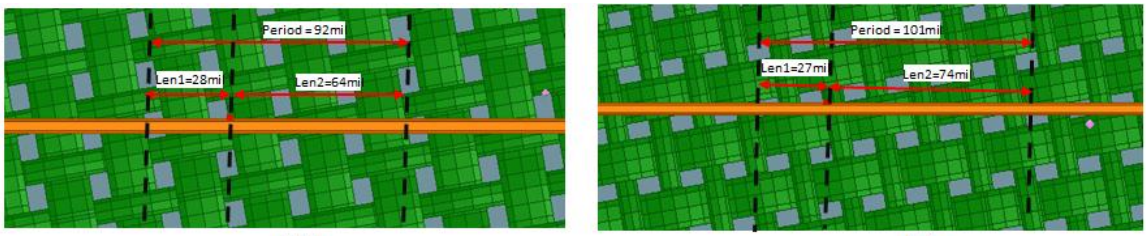

(a) (b)

Figure 8. Unit cell definition of rotated micro strip on layer 6 of test board. Weave type is 1080. (a) 10^0 rotation, (b) 80^0 rotation

Figure 9 validates our simulation model with an overlay plot from a 50GHz VNA measurement and simulated insertion-loss profile of an inch long single ended Microstrip line on a 1080 weave of an ISOLA RTC test board. As in this figure, 10^0 rotated configurations gave the best match to the measurement. This weave orientation was also confirmed from PCB cross-section image measurements.

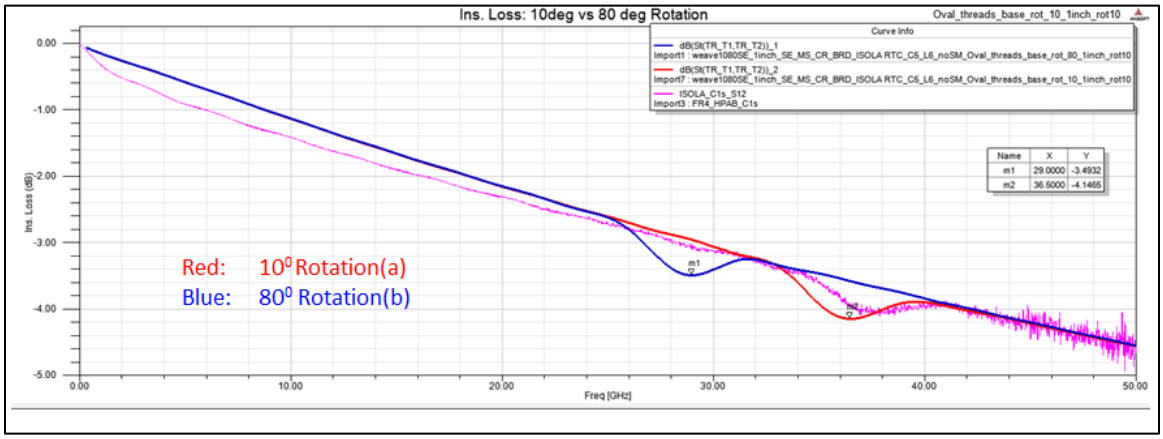

Figure 9. Comparing Simulated S12 of a 1-inch line with two possible rotations.

Characterizing Periodic a Unit cell of a Fiber Weave Model

Solving accurate 3D models presented in the previous section is not very practical for real world transmissions due to intensive computing resource requirements. At the time of this writing, solving fiber weave models with traces longer than three inches needed multiple HPC nodes in order to complete the simulation within a reasonable time. However, just a single unit-cell can be conveniently solved in relatively no time. So we employed a hybrid approach to characterize a single unit cell using 3D EM Simulation

and then apply the periodic transmission line theory to scale it to any given length. This hybrid modeling approach enables us to develop terminal s-parameter models for periodically loaded stripline and microstrip lines by performing 3D or 2D simulation on ports of a unit cell only.

To demonstrate this approach, a strip line trace sandwiched between a symmetric 106-type prepreg was selected as an example. As illustrated in Figure 10, fundamental periodic patterns were identified. A technique to identify an approximate dominant period was proposed by [4]. Once we find an approximate period, we can graphically measure corresponding "weft period" and "warp period" were dimensions as presented in [3, 8] for advanced theoretical calculations.

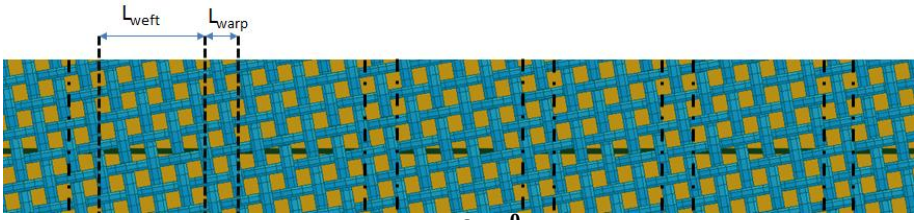

Figure 10. Dominant Periods (MCP) of 10^0 rotated trace on Type-106 weave.

Periodic unit-cells were modeled as two short transmission lines in HFSS as in Figure 10. These two models were solved and R, L, G, and C parameters were computed for each model. The insertion loss for a complete one-inch long transmission line was analytically computed using equation (31). For comparison purposes the complete structure was also solved using a 3D EM simulation tool.

Figure 11is an overlay plot of theoretical calculations and complete 3D EM simulation results of insertion loss for a one-inch single-ended line. In this plot we also included a uniform model (green plot) to capture loss due to all other factors except periodic loading. Then we added the calculated periodic loss profile to the uniform S_{21} to get the compound S_{21}profile (blue plot). As seen from the plot, both theory and simulation (red plot) are matching well at first and second resonances. Using a similar approach, higher frequency resonances can also be superimposed by considering other shorter periods.

In this example we demonstrated that non-periodic transmission line models can be analytically corrected to include periodic effects with adequate accuracy.

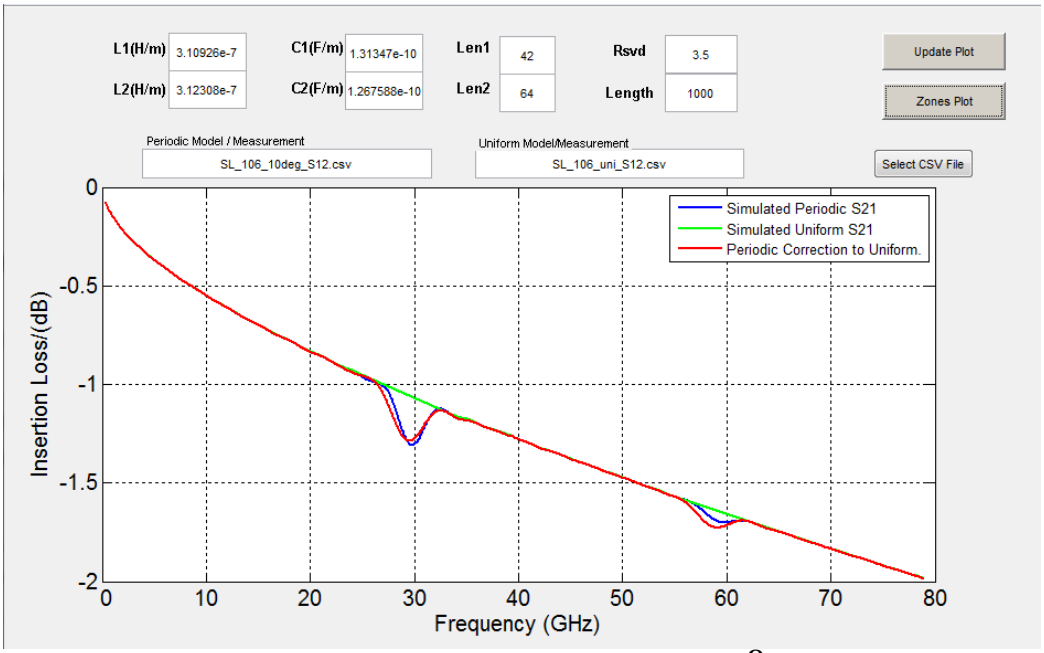

Figure 11. Simulated and calculated resonances on a 10^{O}-rotated trace on 106 weave.

Application to Electromagnetic Field Solvers

Applying the Floquet-Bloch theory and principles to generalized 3D EM field solvers requires that the user will be able to discretize transmission lines into periodic sections. This includes both the fiber weave and the copper trace segments. Figure 12 shows a DDR3 trace routing that is typical for memory DIMM modules. The DDR3 net starts on the bottom and has multiple layer transitions within the PCB.

Due to the non-periodic routing of traces which is common within the industry the author's opinion is the application to 3D EM field solvers would be limited due to the cumbersome overhead of defining individual periodic unit cells. In addition the accuracy for a 3D field solver would be degraded as mutual couplings that were not periodic in nature would be disregarded using this approach.

Applying the Floquet-Bloch theorem to a full-wave hybrid field solver where the trace segments are decomposed from the plane geometries and via transitions could yield positive results for both speed and accuracy. Hybrid solvers utilize a highly efficient modeling technique which analyzes complete power distribution systems along with signal nets for the characterization of entire electronic packages and boards [11]. This includes multilayered power/ground planes containing multiple vias and multi-conductor signal traces. The total electromagnetic fields inside the multilayered structures (packages and boards) are decomposed into parallel-plate and transmission-line modes. Within each parallel plate waveguide region that is formed by a pair of power and ground planes a two dimensional wave equation is formulated and solved using the finite element method. For high speed digital designs only the fundamental, TEM, mode needs to be considered in

these parallel plate waveguide regions. This is due to the high cut-off frequency associated with the higher order modes. Using these restrictions a modified form of Maxwell's equation needs to be solved.

$$\nabla_t \cdot \frac{1}{R + j\omega L} \nabla_t V_p - \quad G + j\omega C \;\; V_p = 0 \tag{34}$$

The scalar unknown, V_p, represents the voltage drop between the planes, and L, C, R, G are respectively the inductance, capacitance, resistance, and conductance per unit area. The symbol ∇_t in (34) represents a two-dimensional gradient/divergence operator. Equation (34) is efficiently solved using a two dimensional finite element algorithm. In addition to the power and ground planes, packages and boards have many signal traces passing between these planes. When a trace is present, the assumption that the electric field is orthogonal to the power and ground planes becomes invalid. Hence, a modal decomposition method is employed to decouple the transmission line TEM mode from the parallel plate mode. The traces between the planes and the microstrip line mode for traces on top/bottom of the package are modeled as admittance (Y) networks by using multi-conductor transmission line theory based on solving the Telegrapher's equation(35):

$$\frac{\partial^2}{\partial_z^2} V_t - \quad R + j\omega L \quad G + j\omega C \;\; V_t = 0 \tag{35}$$

Here V_t is the modal voltage on the trace (a function of the distance parameter z) and R, L, G, and C are the trace parameters per unit length. Other discontinuities in the ground and power planes, such as through-hole signal vias, can be represented by equivalent circuits. The transmission line and via circuit parameters are determined by either analytical formulas or fast quasi-static field solvers. The circuit models for the traces and vias can then be combined with the two-dimensional finite element model of the planes to yield a matrix describing the entire system. With this hybrid methodology, large boards and packages can be solved accurately in a reasonable length of time, even when other three dimensional solver methods become intractable.

Using this type of approach the preprocessor could determine the periodic structures and solve each 2D trace segment as a Floquet-Bloch periodic unit cell thereby applying the fiber weave effect into the entire PCB or PKG extraction. This results of this approach and findings are left for future work.

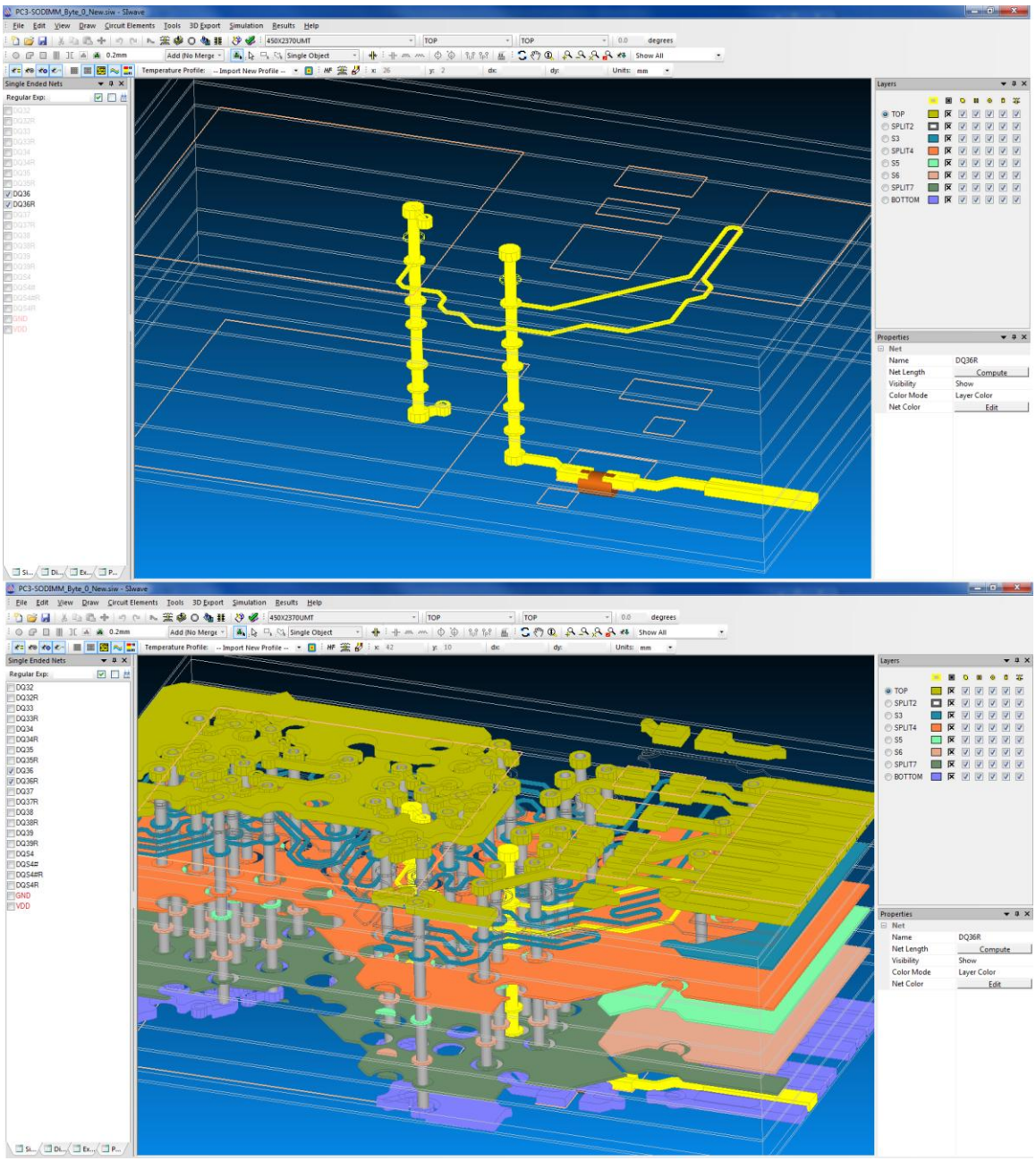

Figure 12: Typical DDR3 trace routing within a PCB. Top picture shows via transitions and trace segments only. Bottom picture shows non-ideal power and ground along with the DDR3 net.

VNA Measurement and Analytical prediction

Figure 12 shows an overlay plot of measured and theoretical insertion-loss profiles for a 5-inch long Microstrip line on a 1080weave of an ISOLA RTC test board. As in previous example only Unit cell models were created in HFSS. Stackup material and trace geometry were closely matched to our test boards on which the measurement was taken. R, L, G, and C parameters were extracted at both ports on the unit cell and periodic

resonances were computed using a software tool developed with Matlab®, scripts and GUIDE® graphical user interface. Overall measured and theoretical insertion-loss plots given in Figure 13 show a good match. Peak resonance frequency is closely matching, but the theoretical formula predicted slightly more loss, which is possibly due to unaccounted losses in the measurement system and irregularities in real fiber bundles.

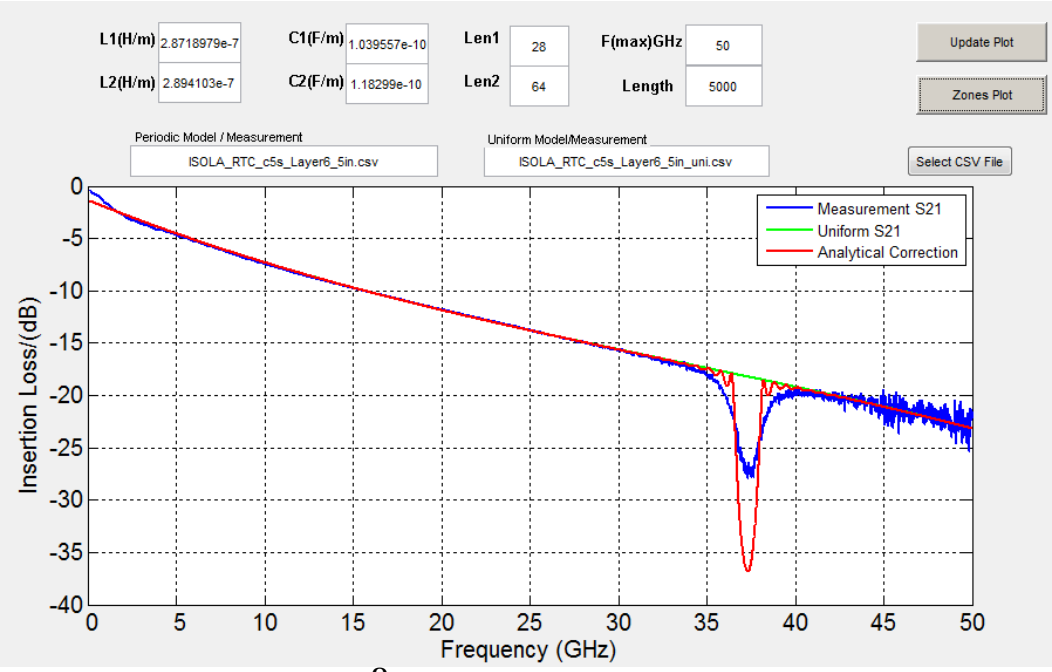

Figure 13. Measured S_{21} of 10^{O} rotated, 5" long Microstrip on layer 6 of test board and computed S_{21}.

High Frequency VNA Measurements

Our 3D EM simulations of realistic fiber weave models and analytical computation technique presented in previous sections predicted correlating periodic resonances. On these 10-degree rotated trace models, we observed the first resonance to be relatively larger (in the neighborhood of 20GHz to 4GHz) and subsequent resonances in higher frequencies to be relatively smaller. Second and higher frequency resonances occurs at very high frequencies (above 50GHz), which are out of the range of the capabilities of most PCB characterization lab instruments.

In order to experimentally verify the predictions discussed above, S-Parameters corresponding to stripline and microstrip test boards fabricated on ISOLA substrates were measured up to 110GHz. S-Parameter measurements of the single ended traces were taken with the state-of-the-art Agilent Performance Network Analyzer (PNA) setup at Intel Labs. This setup extends the frequency sweep capability of the 67GHz Agilent 4-port E8361A/ N4421B PNA to 110 GHz by combining a N5260A millimeter head controller and a pair of millimeter Frequency Extender heads. This measurement setup is

capable of performing 2-port measurements with single frequency range sweep from 10MHz to 110GHz.

A pair of W-Band (110GHz) RF probes was used on both ends of the traces (DUT). These ACP110-A series Air-Coplanar Probes (ACP) were made by Cascade Microtech® to match the 250um pitch ground-signal-ground (GSG) contact points on our test boards. ACP probes use a short 1.0mm air dielectric cable to connect to test ports of waveguide modules. A two-port Line-Reflect-Reflect-Match (LRRM) calibration was performed using Thru, Reflect and Load structures of the precision calibration substrate. A microscopic view of a 110GHz ACP Probe near a 10-degree rotated, non-soldermasked microstrip launch with visible 1080 fiber weaves is shown in Figure 14.

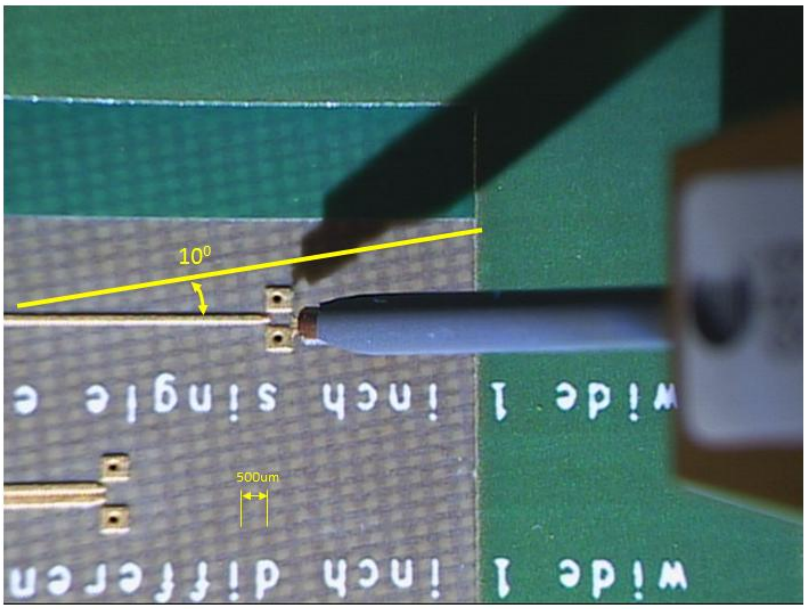

Figure 14. Microscopic Top View of Visible Layer 6 Weaves and 110GHz ACP Probe.

Figure 15 shows an example of an S-Parameter measurement taken on a 3-inch long Microstrip line on ISOLA RTC test board. This measurement confirmed a larger loss around 37GHz. We also confirmed smaller second stop band around 63GHz and a third resonance near 72GHz. These observations are in agreement with our 3D-EM simulations and analytical calculations. Due to excessive loss at higher frequencies, we were only able to get good measurements up to 110GHz on traces shorter than 3 inches.

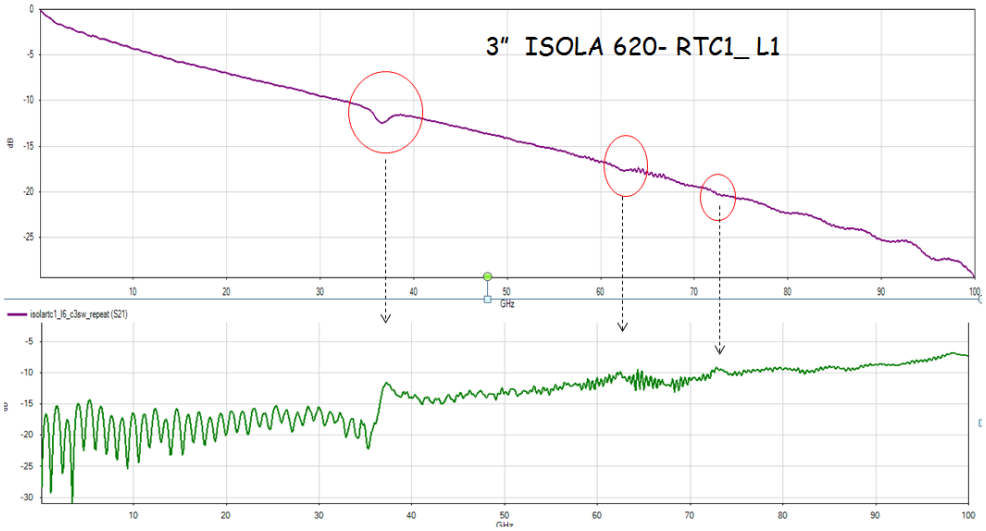

Figure 15. High-Frequency S-Parameter Measurements of a 3" ISOLA/1080 Microstrip.

Summary

High-speed data signals often encounter periodic dielectric conditions along their propagation path. Periodic discontinuities such as fiber weaves can introduce additional loss mechanisms in certain high frequency bands. It is important to take this effects in to account in sub-millimeter wavelength interconnect designs. Modeling real world PCB trace lengths with complete fiber wave structures is not practical due to the need for intensive computing resources. VNA measurement based modeling is also not feasible because, making good measurements needs cost prohibitive equipment to cover a large frequency sweeps with higher dynamic ranges.

In this paper, we have outlined the periodic transmission theory and introduced an analytical technique to compute these additional losses in terms of the channel's periodic properties. We treated PCB fiber weave structures as a periodic medium for propagating waves and applied the analytical formulae to correct PCB trace S-Parameter models to account for periodic loading in addition to all other loss contributions. This modeling technique can be effectively applied to create scalable transmission line models with periodic loading by characterizing just a single unit cell. Analytical approach proposed here can be ubiquitously applied to any periodic structure, which can be distinguished as a cascaded unit cell structure. This technique can also be extended to predict resonances on high speed serial differential trace pairs. Our analytical models are in good agreement with 3D EM simulations and VNA measurements up to 100GHz.

References

1. Jones, Christine Madden. Measurement and Analysis of High Frequency Resonances in Printed Circuit Boards. University of South Carolina Thesis, 2010.
2. Pathmanathan, Priya, Christine Madden Jones, Steven G. Pytel, David L. Edgar, and Paul G. Huray. "Power Loss Due to Periodic Structures in High-speed Packages and Printed Circuit Boards." Proceedings of 18th European Microelectronics Packaging Conference, 2011.
3. Schauer, Martin. "Understanding and Mitigation of Fiber Weave Effects in Striplines." Proceedings of DesignCon 2012.
4. Miller, Jason R. et al., "Additional Trace Loss Due to Glass-Weave Periodic Loading." Proceedings of Annual Designcon Conference, Santa Clara, CA, 2010.
5. Collin, Robert E. Field Theory of Guided Waves. 2nd ed. Wiley-IEEE Press, 1990.
6. Yeh, Pochi, Amnon Yariv, and Chi-Shain Hong. "Electromagnetic Propagation in Periodic Stratified Media I General Theory." Journal of the Optical Society of America 67, no. 4 (1977): 423
7. Chris Herrick, Thomas Buck, and Ruihua Ding. “Simulation Fiber Weave Effect”. (http://pcdandf.com/cms/magazine/95/6187), Printed Circuit Design and Fab, May 2009.
8. Pathmanathan, Priya. "Power Transmission Loss Due To Periodic Loading In Multi-Gigabit Data Signaling Interconnects”. University of South Carolina Dissertation, 2012.
9. Paul G. Huray. The Foundations of Signal Integrity, John Wiley & Sons, Inc. 2010
10. Chip Aware System Design, (http://www.eetimes.com/electrical-engineers/education-training/webinars/4395663/Chip-Aware-System-Design-)
11. S.G. Pytel, S.C. McMorrow, T. Dagostino, S. Polstyanko, W. Thiel, and R. Hall, “Successful Practices for the Modeling of Printed Circuit Boards and Substrates Using Electromagnetic Field Solvers”, 43rd International Symposium on Microelectronics, October 31 – November 4, 2010.